



A synthetic C4 shuttle via the β -hydroxyaspartate cycle in C3 plants

Marc-Sven Roell^a, Lennart Schada von Borzyskowski^{b,1}, Philipp Westhoff^{a,c}, Anastasija Plett^{a,c}, Nicole Paczia^b, Peter Claus^b, Urte Schlueter^a, Tobias J. Erb^{b,d}, and Andreas P.M. Weber^{a,c,2}

^aInstitute of Plant Biochemistry, Heinrich Heine University, 40225 Düsseldorf, Germany; ^bDepartment of Biochemistry and Synthetic Metabolism, Max Planck Institute for Terrestrial Microbiology, 35043 Marburg, Germany; ^cCluster of Excellence on Plant Science, Heinrich Heine University, 40225 Düsseldorf, Germany; and ^dLOEWE Center for Synthetic Microbiology, Philipps-University Marburg, 35043 Marburg, Germany

Edited by Donald R. Ort, University of Illinois at Urbana–Champaign, Urbana, IL, and approved April 7, 2021 (received for review November 2, 2020)

Plants depend on the enzyme ribulose-1,5-bisphosphate carboxylase/oxygenase (Rubisco) for CO₂ fixation. However, especially in C3 plants, photosynthetic yield is reduced by formation of 2-phosphoglycolate, a toxic oxygenation product of Rubisco, which needs to be recycled in a high-flux-demanding metabolic process called photorespiration. Canonical photorespiration dissipates energy and causes carbon and nitrogen losses. Reducing photorespiration through carbon-concentrating mechanisms, such as C4 photosynthesis, or bypassing photorespiration through metabolic engineering is expected to improve plant growth and yield. The β -hydroxyaspartate cycle (BHAC) is a recently described microbial pathway that converts glyoxylate, a metabolite of plant photorespiration, into oxaloacetate in a highly efficient carbon-, nitrogen-, and energy-conserving manner. Here, we engineered a functional BHAC in plant peroxisomes to create a photorespiratory bypass that is independent of 3-phosphoglycerate regeneration or decarboxylation of photorespiratory precursors. While efficient oxaloacetate conversion in *Arabidopsis thaliana* still masks the full potential of the BHAC, nitrogen conservation and accumulation of signature C4 metabolites demonstrate the proof of principle, opening the door to engineering a photorespiration-dependent synthetic carbon-concentrating mechanism in C3 plants.

photosynthesis | photorespiration | synthetic biology | crop improvement | C4

Future agriculture must reconcile sustainability with increased productivity to supply global food demands that will have doubled by 2050 (1, 2). To fulfill this goal, agricultural yields will have to increase annually by 2.4%. However, yields currently plateau at a 1% annual increase in major food crops [i.e., maize, rice, and wheat (3, 4)]. In high-yielding crop varieties, both plant architecture and the harvest index—the fraction of total energy in plant biomass contained in the harvestable organs—approach their theoretical limits (5).

Synthetic biology-based approaches are focusing on improving the carbon conversion efficiency of plants that currently only reaches 20% of its theoretical potential (5, 6). Synthetic biology applies engineering principles to biological systems and multiple synthetic biological solutions to improve the carbon conversion efficiency of plants were recently proposed (6, 7). These include pathways for improved CO₂ fixation (Rubisco based and Rubisco independent), such as the crotonyl-coenzyme A (CoA)/ethylmalonyl-CoA/hydroxybutyryl-CoA cycle (8, 9), photorespiratory bypasses, including the Tartonyl-CoA (TaCo) pathway and a modified 3-hydroxypropionate bicycle (10), as well as synthetic carbon-concentrating mechanisms. Altogether, these proposed solutions showcase the potential of plant synthetic biology to increase productivity and sustainability of future agriculture beyond the realms of natural evolution (7, 11, 12).

Natural carbon-concentrating mechanisms boost carbon fixation by concentrating CO₂ at the site of Rubisco and have independently evolved in cyanobacteria [carboxysomes (13)], green algae [pyrenoids (14)], and plants [C4 photosynthesis, single-cell C4 photosynthesis, and crassulacean acid metabolism (7)]. In C4

photosynthesis, primary CO₂ fixation is spatially separated from Rubisco. First, CO₂ is captured into a C4 acid via phosphoenolpyruvate carboxylase (PEPC) in mesophyll cells, and this C4 acid is then decarboxylated in bundle sheath cells, where Rubisco is located. The increase in the local CO₂ concentration reduces the oxygenation reaction of Rubisco as well as the subsequent process of photorespiration (15). Consequently, implementation of C4 photosynthesis into C3 plants has received much attention to increase yield in crop plants that experience photorespiration (16, 17).

Another target to improve plant growth is photorespiration itself. During natural photorespiration, the Rubisco oxygenation product 2-phosphoglycolate is recycled back into 3-phosphoglycerate. However, natural photorespiration comes with the loss of up to 30% of previously fixed carbon (18), release of nitrogen, and the dissipation of energy (19), which has led to the engineering of photorespiratory bypasses to mitigate the deleterious effects of photorespiration. In particular, glycolate, formed by dephosphorylation of 2-phosphoglycolate, has been considered an ideal starting

Significance

Photorespiration is essential for photosynthesis in an oxygen-containing atmosphere. By mass flow, photorespiration is exceeded only by photosynthetic carbon assimilation. Photorespiration, initiated by the oxygenation reaction of Rubisco, is a major constraint on the photosynthetic efficiency of C3 plants and consequently on crop yield. Mitigating the negative effects of photorespiration holds potential for yield increases and contributes to achieving food and energy security for a growing population. This work presents a synthetic bypass to natural photorespiration (i.e., the conversion of photorespiratory glycolate into a C4 compound via a recently discovered microbial glycolate assimilation pathway, the β -hydroxyaspartate cycle [BHAC]). Simultaneous expression of four enzymes of microbial origin in the land plant model *Arabidopsis thaliana* enables efficient glycolate conversion into BHAC products.

Author contributions: M.-S.R., L.S.v.B., P.W., A.P., T.J.E., and A.P.M.W. designed research; M.-S.R., L.S.v.B., P.W., A.P., N.P., P.C., and U.S. performed research; M.-S.R., L.S.v.B., P.W., A.P., U.S., T.J.E., and A.P.M.W. analyzed data; and M.-S.R., L.S.v.B., P.W., A.P., T.J.E., and A.P.M.W. wrote the manuscript.

Competing interest statement: The Heinrich Heine University and the Max-Planck-Gesellschaft zur Förderung der Wissenschaften are the patent applicants for European patent application no. EP 19190404.4, which includes a method for the production of plants with altered photorespiration and improved CO₂ fixation due to the BHAC.

This article is a PNAS Direct Submission.

This open access article is distributed under [Creative Commons Attribution License 4.0 \(CC BY\)](https://creativecommons.org/licenses/by/4.0/).

¹Present address: Institute of Biology Leiden, Leiden University, Leiden, 2333 BE, The Netherlands.

²To whom correspondence may be addressed. Email: andreas.weber@hhu.de.

This article contains supporting information online at <https://www.pnas.org/lookup/suppl/doi:10.1073/pnas.2022307118/-DCSupplemental>.

Published May 17, 2021.

metabolite for several photorespiratory bypasses (7, 20). Photorespiratory bypasses that recycle glycolate into 3-phosphoglycerate by the cyanobacterial “glycerate pathway” or oxidize glycolate in the chloroplast have already shown growth benefits in greenhouse-grown *Arabidopsis thaliana* (21, 22) and tobacco and rice in field experiments (23, 24). However, all of these bypasses still release CO₂, which limits their efficiency compared to natural photorespiration.

Recently, the β-hydroxyaspartate cycle (BHAC) was described as primary pathway of glycolate assimilation in marine proteobacteria (25). In this pathway, glycolate is first oxidized into glyoxylate, which is further converted into oxaloacetate (OAA) in four enzymatic steps, the core of the BHAC (Fig. 1). Notably, the BHAC enables the direct formation of a C₄ compound from glycolate, without the loss of carbon and nitrogen, which renders the BHAC more efficient than natural photorespiration and all other photorespiration bypasses engineered in vivo so far.

Here, we demonstrate the implementation of the BHAC in *A. thaliana* (*Arabidopsis*) peroxisomes. We validate activity of the BHAC in planta by demonstrating β-hydroxyaspartate (BHA) formation under photorespiratory conditions. Furthermore, we show improved nitrogen conservation through the BHAC, which results in reduced free ammonia levels compared to natural photorespiration. We also determine the metabolic fate of BHAC-derived OAA and outline a strategy to use BHAC-derived OAA to establish a synthetic C₄ cycle in C₃ plants. Altogether, our proof-of-principle study demonstrates an approach to turn a photorespiratory bypass into a carbon concentrating mechanism by synergistically coupling photorespiration and C₄ metabolism. By engineering two of the main targets in primary plant metabolism, this study creates opportunities for improved agricultural productivity in the future.

Results

BHAC Implementation in Plant Peroxisomes. Photorespiratory glycolate is converted to glyoxylate in peroxisomes. Since glyoxylate is the starting substrate of the BHAC, we implemented the BHAC in the peroxisomal matrix. The four BHAC enzymes, aspartate:glyoxylate aminotransferase (AGAT, Enzyme Commission [EC]: 2.6.1.35), β-hydroxyaspartate aldolase (BHAA, EC: 4.1.3.41), β-hydroxyaspartate dehydratase (BHAD, EC: 4.3.1.20), and iminosuccinate reductase (ISR), were targeted to plant peroxisomes by fusion of a peroxisomal target signal (PTS). AGAT,

BHAD, and ISR were C terminally fused with PTS1 (26). BHAA was fused N terminally with the PTS2 from *Arabidopsis* citrate synthase 3 [At2g42790 (26)]. Peroxisomal localization of the four BHAC enzymes was confirmed by fluorescence colocalization with a peroxisomal marker in *Nicotiana benthamiana* protoplasts and extrapolated for BHAC implementation in *Arabidopsis* (Fig. 2A).

We selected four *Arabidopsis* photosynthetic promoters [Rubisco small subunit 1B, 2B, 3B (27), and chlorophyll A/B-binding protein 1 (28)] to restrict BHAC enzyme expression to photosynthetic tissue (*SI Appendix*, Fig. S1). Furthermore, we hypothesized that reduced conversion of glyoxylate to glycine would enhance metabolic flux through the BHAC. Besides *Arabidopsis* wild-type *Col-0* (WT), we therefore selected the photorespiratory *ggt1-1* mutant as background for BHAC implementation. The *ggt1-1* mutant is deficient in the peroxisomal glutamate glyoxylate aminotransferase 1 (29) and shows a strong photorespiratory phenotype, which allowed us to screen for the function of the BHAC via a convenient visual readout.

In total, 14 and 11 primary transformants that harbor the complete transfer DNA insertion were identified in the WT and *ggt1-1* background, respectively. Out of these two independent lines, each were established in the WT (*Col::BHAC #1* and *#2*) and *ggt1-1* background, respectively (*ggt1-1::BHAC #1* and *#2*, *SI Appendix*, Fig. S1), based on immunoblot analysis to verify expression of all four BHAC enzymes in the transgenic lines (*SI Appendix*, Fig. S1). We quantified activity of each BHAC enzyme in mature rosette leaf extracts of 4-wk-old air-grown plants by enzyme activity assays (Fig. 2B). AGAT was highest in both WT and *ggt1-1* backgrounds compared to BHAA and BHAD activity (Fig. 2B). Iminosuccinate is a labile product formed by BHAD (25). To demonstrate functional expression of ISR, we therefore quantified the rate of ¹⁵N incorporation into L-aspartate, which confirmed ISR activity in BHAC plants (Fig. 2B). In summary, these experiments confirmed the successful expression of all enzymes in planta.

Peroxisomal BHAC Functions as Photorespiratory Bypass. Next, we verified that the peroxisomal BHAC functions as photorespiratory bypass by steady-state metabolomics on green tissue of 14-d-old seedlings either grown in CO₂-enriched air (3,000 ppm CO₂, high carbon, HC), ambient air (400 ppm CO₂, ambient carbon, AC), or shifted from CO₂-enriched to ambient air 3 d before sampling (Shift, Fig. 3). Our metabolomics analysis included the BHAC

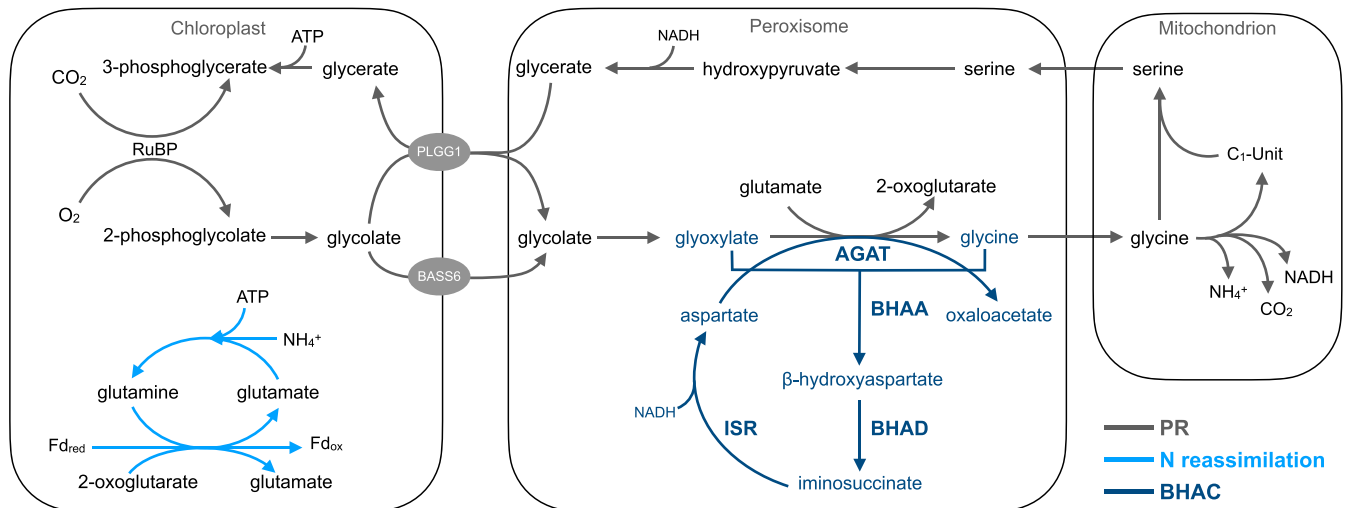


Fig. 1. The BHAC as photorespiratory bypass in plant peroxisomes. A schematic representation of plant photorespiration (PR) and photorespiratory nitrogen (N) reassimilation (light blue) and the BHAC (dark blue) AGAT, BHAA, BHAD, ISR, GGT1, ribulose-1,5-bisphosphate (RuBP), plastidial glycolate/glycerate transporter 1 (PLGG1), and bile acid sodium symporter 6 (BASS6).

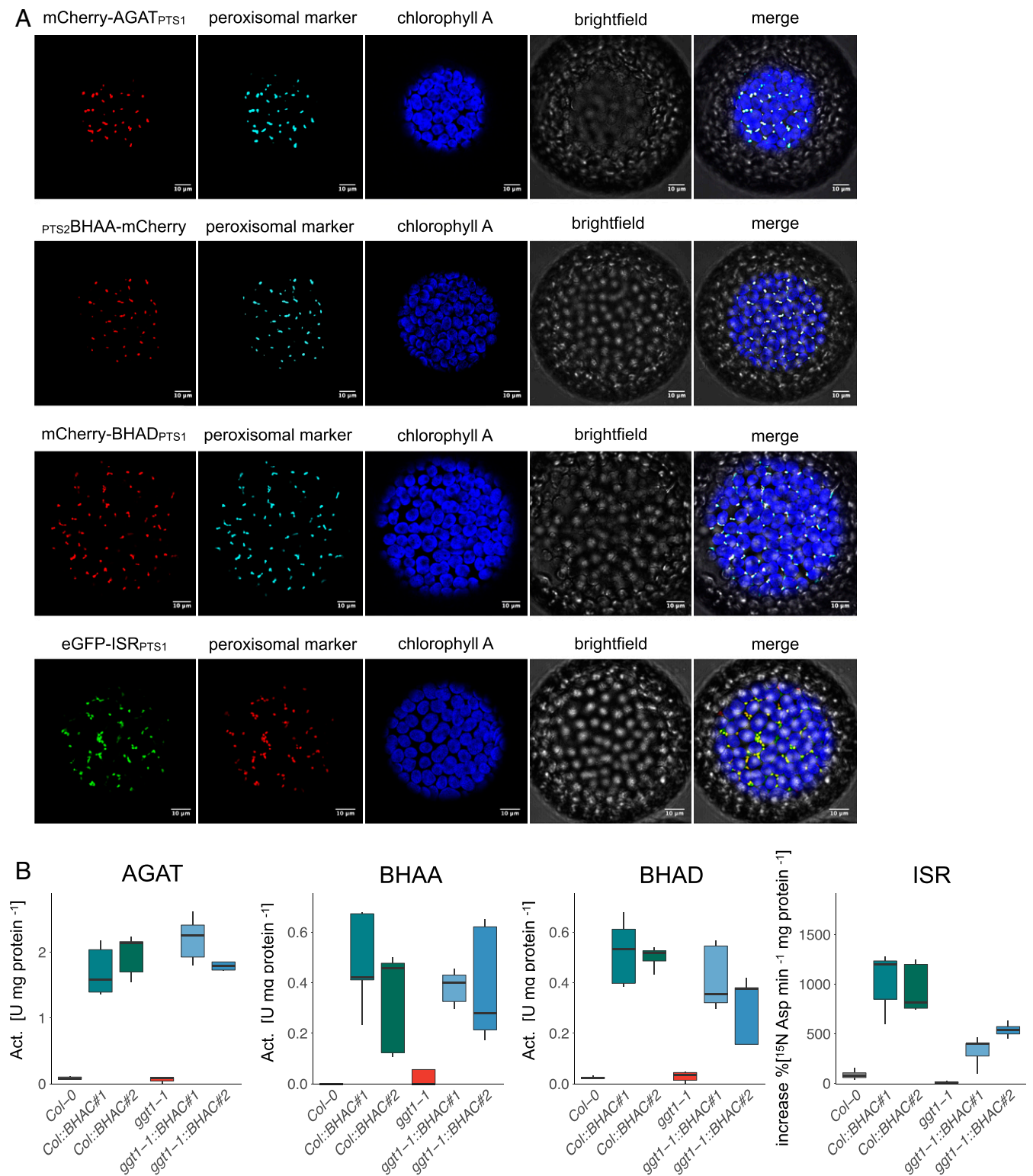


Fig. 2. Peroxisomal targeting and enzyme activity of the BHAC. (A) Fluorescent fusion constructs for each BHAC enzyme were coinfiltrated with a peroxisomal marker in *N. benthamiana* leaves, and protoplasts were analyzed by confocal microscopy 2 d postinfection. Both the peroxisomal targeting sequence (subscripted) and the fluorescent fusion protein are indicated based on the protein N- or C-terminal position. AGAT, BHAA, BHAD, and ISR. Blue: chlorophyll A autofluorescence, Peroxisomal marker: cyan fluorescent protein or mCherry (only for ISR) with C-terminal PTS1 (Scale bar, 10 μm). (B) BHAC enzyme activity in *Arabidopsis* mature rosette leaf extracts of 4-wk-old air-grown plants. For the ISR assay, the percentual ^{15}N label enrichment into aspartate was quantified over time. $n = 3$.

intermediates BHA and glycine; malate, produced by reduction of BHAC-derived OAA by peroxisomal NAD-dependent MDH (30), as well as aspartate, which can be regarded both as BHAC intermediate and product of OAA transamination (Fig. 3).

BHA is a unique metabolite of the BHAC and not naturally present in *Arabidopsis* (Fig. 3 A and B). We analyzed analytical standards of BHA diastereomers via gas chromatography–time-of-flight mass spectrometry (GC/MS Q-TOF) to annotate BHA according to the electron impact mass spectral fragmentation pattern (SI Appendix, Fig. S2). As expected, BHA-specific fragments were neither detected in WT nor in *ggt1-1* controls under all conditions tested. In contrast, BHA could be detected in plants carrying the BHAC (SI Appendix, Fig. S3). However, relative quantification revealed that BHA was only detectable when plants were grown in ambient air or shifted from CO₂-enriched to ambient air but not in CO₂-enriched air (Fig. 3 A and B). This confirmed function of the BHAC in planta and suggested that BHA formation is exclusively linked to photorespiratory conditions.

Glycine levels decreased twofold in both *Col::BHAC* lines, which is consistent with glycine conversion into BHA by BHAA under photorespiratory conditions in ambient air (Fig. 3C). In the *ggt1-1* mutant total glycine levels were 10-fold lower compared to WT (29) and remained unaltered in *ggt1-1::BHAC* plants (Fig. 3C) despite partial restoration of peroxisomal glyoxylate to glycine conversion through a promiscuous aminotransferase activity of AGAT in the *ggt1-1* mutant (Fig. 3C). In line with BHAC activity, aspartate and malate levels were elevated sixfold and twofold, respectively, in ambient air-grown BHAC plants of both background genotypes compared to WT (Fig. 3C). Together, the formation and accumulation of BHAC-specific metabolites exclusively in photorespiratory conditions demonstrated that the peroxisomal BHAC indeed functions as photorespiratory bypass.

The BHAC Reshapes Carbon and Nitrogen Metabolism. To better understand the metabolic implications of the BHAC, we generated metabolite profiles for all four BHAC lines (BHAC plants) and their background genotypes at different CO₂ concentrations (HC, AC, and Shift; SI Appendix, Fig. S4). Growth condition-dependent principal component analysis revealed that the metabolic profiles of BHAC plants are clearly distinct from their background genotypes (Fig. 4A) and that all BHAC plants cluster together, independent of their genetic background under photorespiratory conditions (AC or Shift; Fig. 4A). Notably, we did not observe such clustering of genotypes under HC (Fig. 4A), which is consistent with the observation that the BHAC is only active under photorespiration.

We further focused on the metabolite profile of BHAC plants in comparison to the WT and *ggt1-1* mutant backgrounds grown under photorespiratory conditions in ambient air (Fig. 4B). In plant photorespiration mitochondrial glycine decarboxylase is the major hub of carbon and nitrogen losses (19, 31). Nitrogen conservation by the BHAC is assumed to prevent mitochondrial ammonia release and avoid chloroplastic nitrogen reassimilation by glutamine synthase. Consequently, cellular free ammonia levels were reduced on average by 20% in ambient air-grown BHAC plants compared to WT under photorespiratory conditions (Fig. 4C). Furthermore, ambient air-grown BHAC plants accumulated soluble amino acids that are either involved in the urea cycle (glutamate and ornithine) or depend on OAA-derived carbon skeletons (lysine and methionine; Fig. 4B).

Besides peroxisomal reduction to malate, three further routes of OAA assimilation are theoretically possible that are all coupled to the direct export of OAA from the peroxisome (32). Cytosolic phosphoenolpyruvate carboxykinase 1 (PCK1) could decarboxylate OAA to phosphoenolpyruvate [PEP (33)]. PEP is then used either for gluconeogenesis or converted into pyruvate by pyruvate kinase [PK (34)]. The accumulation of pyruvate

strongly indicated that the cytosolic PK route is active in BHAC plants and that PEP is not channeled into gluconeogenesis, which was supported by reduced glucose and fructose levels in the same plants (Fig. 4B). In addition to cytosolic decarboxylation, OAA could also be transported into mitochondria, where it could fuel the mitochondrial tricarboxylic acid (TCA) cycle. Accumulation of citrate in ambient air-grown BHAC plants suggested that this route was also active, eventually in combination with an increased flux of pyruvate into the TCA cycle (Fig. 4B).

To further validate that reshaping of the metabolome in BHAC plants is caused by an active BHAC and not AGAT alone, we complemented the *ggt1-1* mutant with AGAT under control of the chlorophyll A/B-binding protein 1 promoter, which was also used for AGAT expression in *ggt1-1::BHAC* plants (SI Appendix, Fig. S5). Steady-state metabolomics on plants grown under photorespiratory conditions in ambient air revealed that AGAT expression was not sufficient to cause the distinct metabolome signature of BHAC plants. Instead, AGAT expression only restored canonical photorespiration, probably by utilizing aspartate as amino donor for the peroxisomal transamination reaction (SI Appendix, Fig. S5).

In summary, these experiments showed that the BHAC is active under photorespiratory conditions and reshapes the metabolome in plants by altering nitrogen metabolism (amino acid accumulation and free ammonia reduction) and OAA utilization in the cytosol and/or mitochondrial TCA cycle.

The BHAC Reduces Plant Growth by Impaired Photosynthesis in the WT Background. Despite carbon and nitrogen conservation by the BHAC, *Col::BHAC* plants are reduced in growth compared to WT controls in ambient air (Fig. 5A and SI Appendix, Fig. S6). Rosettes of 4-wk-old air-grown *Col::BHAC* plants are decreased by 70% in area and 50% in diameter (SI Appendix, Fig. S7). However, BHAC implementation in the *ggt1-1* mutant partially suppressed the photorespiratory phenotype of the mutant (Fig. 5A) and growth was comparable to *Col::BHAC* plants (SI Appendix, Fig. S7). In CO₂-enriched air, growth of BHAC plants was not altered compared to the background genotype (Fig. 5A and SI Appendix, Fig. S7).

In order to test the hypothesis that reduced plant growth is caused by suppressed photorespiratory 3-phosphoglycerate regeneration in BHAC plants, we analyzed steady-state levels of phosphorylated intermediates in green tissue of 14-d-old air-grown plants (Fig. 5B and SI Appendix, Fig. S8). Whereas 2-phosphoglycolate levels were not significantly altered between all genotypes, the 3-phosphoglycerate levels were reduced in BHAC plants compared to WT and notably very similar to the *ggt1-1* mutant, impaired in photorespiratory 3-phosphoglycerate regeneration (Fig. 5B). In addition, in BHAC plants, 3-phosphoglycerate levels were similar to the *ggt1-1* mutant, impaired in photorespiratory 3-phosphoglycerate regeneration (Fig. 5B). Furthermore, sedoheptulose-7-phosphate, an intermediate of the Calvin-Benson-Bassham cycle (CBBC), showed reduced levels in BHAC plants, whereas ribose/ribulose-5-phosphate levels were not altered (Fig. 5B). We directly assessed the photosynthetic capacity of BHAC plants and generated A/C_i curves, the rate of CO₂ assimilation (A) in relation to intercellular CO₂ concentration (C_i) under saturating light (1,000 μmol · s⁻¹ · m⁻²), by leaf gas exchange measurements of 6-wk-old ambient air-grown plants (SI Appendix, Fig. S9). Based on the A/C_i curve, we determined the CO₂ compensation point (CCP), a net quotient of zero for photosynthetic CO₂ assimilation and respiratory CO₂ release (35). *Col::BHAC* plants displayed an increased CCP compared to WT (Table 1). The *ggt1-1* mutant itself has a higher CCP, and the BHAC did not significantly alter the CCP in this photorespiratory mutant (Table 1). In addition, the maximal assimilation rate at saturated CO₂ (A_{max}) and the initial slope as in vivo measure of the carboxylation efficiency were inferred from the A/C_i curves (36). Compared to WT, both A_{max} and initial slope were reduced

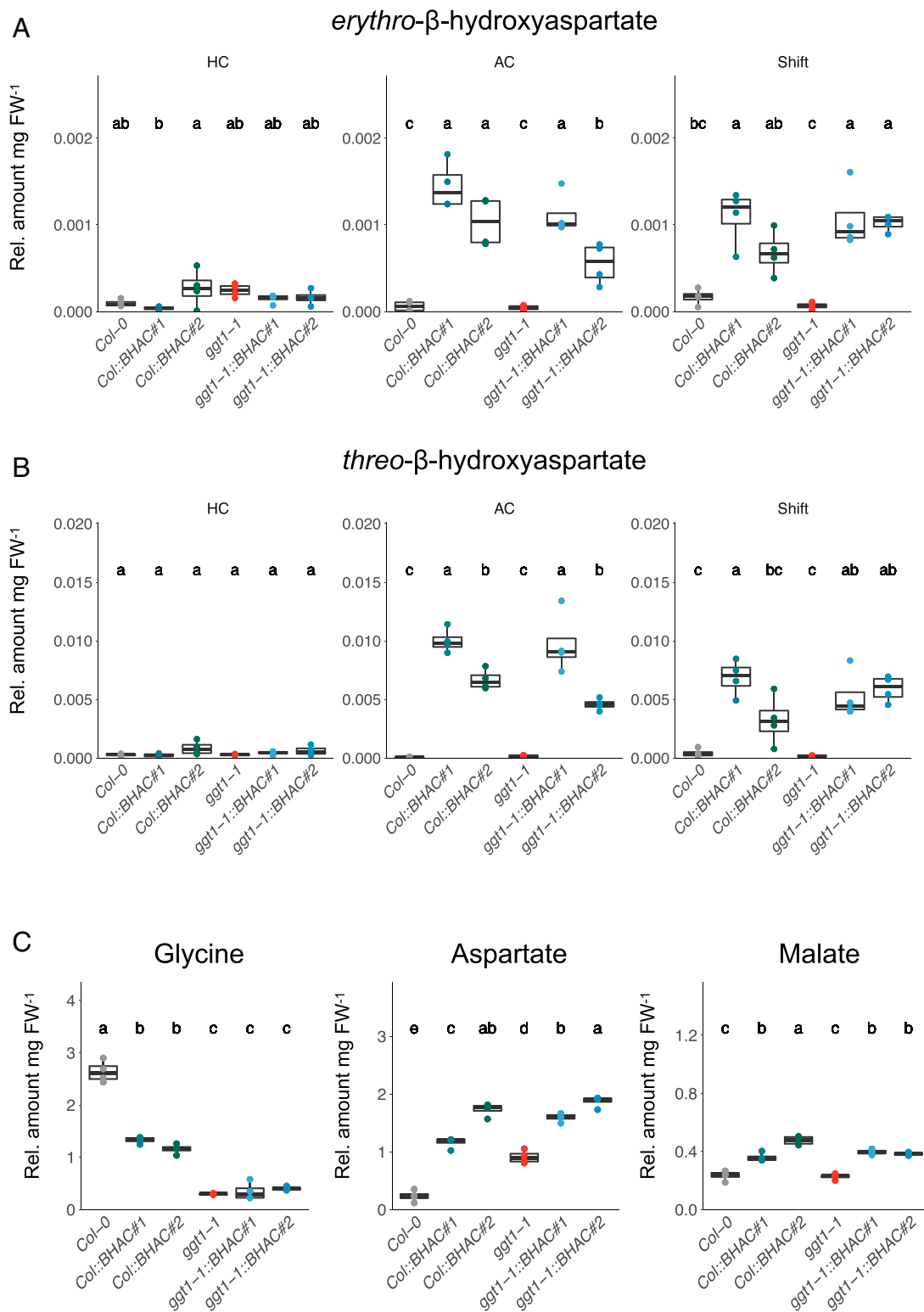


Fig. 3. The BHAC functions as photorespiratory bypass. (A and B) Relative metabolite levels per mg fresh weight (FW) of *in vivo* *erythro*- β -hydroxyaspartate (A) and *threo*- β -hydroxyaspartate (B) formation in BHAC plants. Green tissue of 14-d-old seedlings was harvested in the middle of the light phase. The plants were grown either in CO₂-enriched air (3,000 ppm CO₂, HC), ambient air (400 ppm CO₂, AC), or shifted from HC to AC 3 d prior to harvest (Shift). (C) Relative metabolite levels per mg FW of glycine, aspartate, and malate in BHAC plants grown in ambient air. Each box-whisker plot represents the 25th and 75th percentiles and whiskers the 10th and 90th percentile. The median is indicated as a crossbar. One-way ANOVA with a post hoc Tukey honest significant difference test was used for statistical analysis. The different letters indicate significant differences between genotypes at $P < 0.05$. $n = 4$.

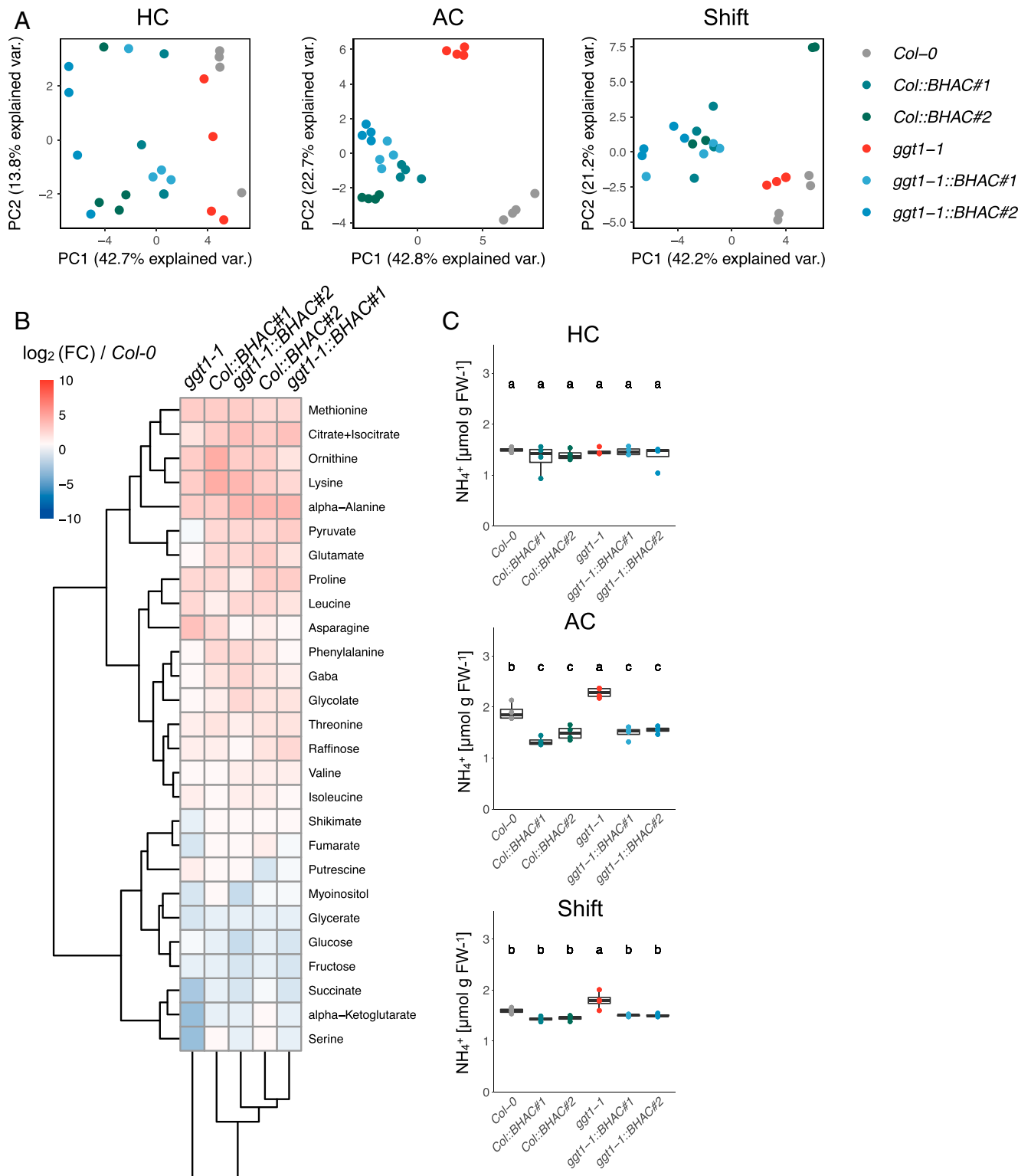


Fig. 4. The BHAC reshapes the plant metabolome. Metabolite profiles were generated using green tissue of 14-d-old seedlings grown either at 3,000 (HC), 400 (AC), or shifted from 3,000 to 400 ppm CO_2 3 d (Shift) prior to harvest at the middle of the light phase. (A) Principal component analysis of the metabolome profiles. (B) Metabolome profiles of AC grown plants. The \log_2 fold change (FC) was calculated compared to wild-type *Col-0* and clustered based on Pearson correlation. (C) Quantification of free ammonium in BHAC plants. Each box-whisker plot represents the 25th and 75th percentiles and whiskers the 10th and 90th percentile. The median is indicated as a crossbar. One-way ANOVA with a post hoc Tukey honest significant difference test was used for statistical analysis. The different letters indicate significant differences between genotypes at $P < 0.05$. $n = 4$ biological replicates measured in technical triplicates.

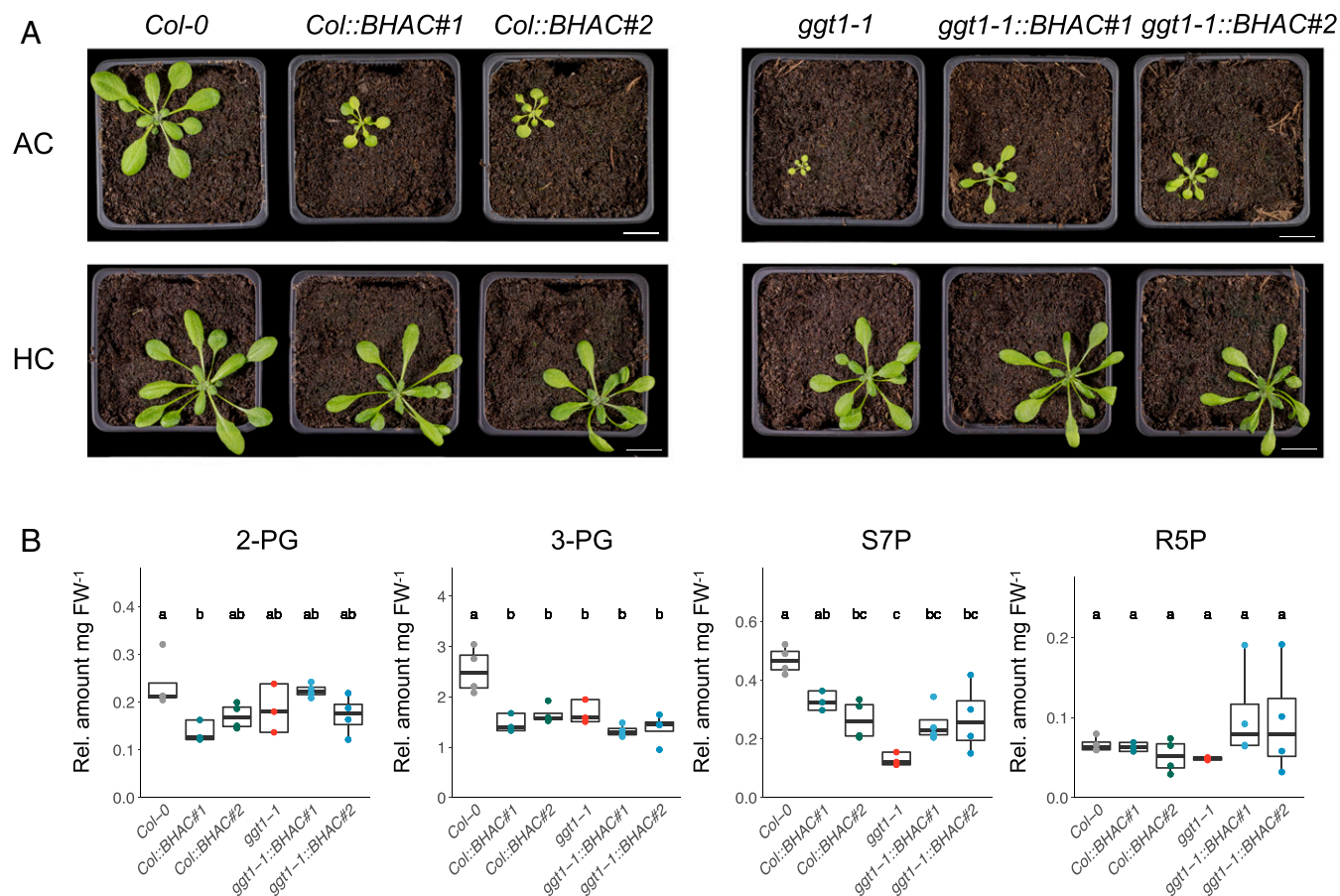


Fig. 5. The BHAC reduces plant growth in air by impaired photosynthesis. (A) Representative images of BHAC plants in ambient air (400 ppm CO₂, AC) or CO₂-enriched air (3,000 ppm CO₂, HC). The images were taken 28 d after transfer to light (Scale bar, 2 cm). (B) Relative levels of phosphorylated metabolites per mg fresh weight (FW) of 2-phosphoglycolate (2-PG), 3-phosphoglycerate (3-PG), seduheptulose-7-phosphate (S7P), and ribulose/ribose-5-phosphate (R5P) in BHAC plants grown in ambient air. Each box-whisker plot represents the 25th and 75th percentiles and whiskers the 10th and 90th percentile. The median is indicated as a crossbar. One-way ANOVA with a post hoc Tukey honest significant difference test was used for statistical analysis. The different letters indicate significant differences between genotypes at $P < 0.05$. $n \geq 3$.

by 25% in *Col::BHAC* plants, while they behaved comparably in *ggt1-1::BHAC* plants (Table 1). Remarkably, neither dark respiration, assessed by light response curve measurements at constant CO₂ (400 μ bar) nor the CCP under low-oxygen conditions (4% O₂) were altered across all genotypes, except a slightly elevated CCP in *ggt1-1::BHAC#2* plants (Table 1 and *SI Appendix*, Fig. S9). Western blot analysis of the Rubisco large subunit and the Rieske-Fe protein demonstrated that the reduced initial slope and A_{\max} in BHAC plants was not caused by altered protein content of these enzymes (*SI Appendix*, Fig. S10).

Discussion

An estimated loss of 30% photosynthetically fixed carbon define photorespiration as a limiting factor of plant growth. However, photorespiratory bypasses can address this issue and improve plant yield (6, 12). The recently described BHAC, naturally found in marine proteobacteria, allows the direct conversion of glyoxylate into OAA, providing options to assimilate photorespiratory glyoxylate without the loss of carbon and nitrogen (25). Here, we report on engineering a functional BHAC in *Arabidopsis* peroxisomes to demonstrate a photorespiratory bypass independent

Table 1. Physiological parameters of BHAC plants

	CCP ($\mu\text{mol} \cdot \text{mol}^{-1}$)	A_{\max} ($\mu\text{mol CO}_2 \text{ m}^{-2} \cdot \text{s}^{-1}$)	A/C_i slope ($\text{mol} \cdot \text{m}^{-2} \cdot \text{s}^{-1}$)	R_{dark} ($\mu\text{mol CO}_2 \text{ m}^{-2} \cdot \text{s}^{-1}$)	CCP 4% O ₂ ($\mu\text{mol} \cdot \text{mol}^{-1}$)
<i>Col-0</i>	61.17 \pm 2.5 ^b	16.52 \pm 2.2 ^a	0.045 \pm 0.005 ^a	-1.07 \pm 0.2 ^a	15.8 \pm 3.3 ^b
<i>Col::BHAC#1</i>	71.20 \pm 3.3 ^{ab}	12.36 \pm 1.5 ^b	0.035 \pm 0.003 ^{ab}	-0.82 \pm 0.1 ^a	17.3 \pm 0.7 ^{ab}
<i>Col::BHAC#2</i>	73.53 \pm 3.7 ^a	10.82 \pm 2.2 ^b	0.031 \pm 0.007 ^{bc}	-0.81 \pm 0.1 ^a	19.7 \pm 1.7 ^{ab}
<i>ggt1-1</i>	80.20 \pm 4.2 ^a	13.52 \pm 1.0 ^{ab}	0.021 \pm 0.004 ^c	-0.94 \pm 0.2 ^a	19.7 \pm 0.6 ^{ab}
<i>ggt1-1::BHAC#1</i>	77.98 \pm 3.6 ^a	11.8 \pm 1.1 ^b	0.030 \pm 0.002 ^{bc}	-0.78 \pm 0.2 ^a	19.8 \pm 2.2 ^{ab}
<i>ggt1-1::BHAC#2</i>	77.58 \pm 9.8 ^a	10.35 \pm 1.4 ^b	0.026 \pm 0.005 ^{bc}	-1.02 \pm 0.3 ^a	22.8 \pm 2.4 ^a

The CCP, A_{\max} , and the slope were determined from the A/C_i curves (*SI Appendix*, Fig. S8). Dark respiration (R_{dark}) was determined from the light response curves, and the O₂ dependency of the CCP was determined at low oxygen concentrations (4%). One-way ANOVA with a post hoc Tukey honest significant difference test was used for statistical analysis. The different superscript letters indicate significant differences between genotypes at $P < 0.05$. $n \geq 3$. Shown are mean \pm SD.

of 3-phosphoglycerate regeneration or decarboxylation of a photorespiratory precursor.

Redirecting the metabolic flux toward a synthetic pathway was demonstrated by combining transcriptional suppression of the plastidial glycolate/glycerate transporter 1 with chloroplastic glycolate decarboxylation in field-grown tobacco plants (23). Similarly, implementing the BHAC in the *ggt1-1* mutant to push pathway flux improved plant growth compared to the mutant background. In plant peroxisomes, the BHAC bypasses the mitochondrial glycine decarboxylase complex that would otherwise release ammonia during photorespiration (Fig. 1). Ammonia reassimilation by passive transport to the chloroplast and refixation by the glutamine synthetase 2/ferredoxin-dependent glutamine:oxoglutarate aminotransferase complex (GS2/Fd-GOGAT) is an integral part of photorespiration (19, 37). Based on the metabolite profiles, we hypothesize three metabolic adaptations that compensate the impaired nitrogen shuttle in BHAC plants. A general response upon impaired GS2/Fd-GOGAT-dependent nitrogen assimilation is the use of cytosolic glutamine synthetases and glutamate dehydrogenases (38). Furthermore, excess nitrogen is stored in the urea cycle (39) and the ornithine–citrulline shuttle that might underpin mitochondrial chloroplastic nitrogen exchange (40). Finally, BHAC-derived OAA can be directly converted into aspartate by aspartate aminotransferase (41). Produced aspartate is used for chloroplastic de-novo biosynthesis of amino acids dependent on C4-carbon skeletons, in particular lysine, threonine, and methionine, that accumulate in BHAC plants [Fig. 4 (42, 43)]. This implies that the BHAC functions as a nitrogen-conserving pathway and allows rerouting of photorespiratory glycolate into amino acids.

In contrast to previous photorespiratory bypasses (21–24), the BHAC also alters the carbon stoichiometry of photorespiration. C3 plants depend on the regeneration of 3-PGA by photorespiration, which is exemplified by the strong phenotype of several photorespiratory mutants (29, 44–46). In BHAC plants, glycolate is directly converted into OAA, and the reduced carboxylation efficiency (initial slope) and A_{\max} are caused by lowered metabolic flux in the 3-phosphoglycerate–regenerating branch of photorespiration in the WT background and comparable to the photorespiratory *ggt1-1* mutant (Fig. 5B and Table 1).

Whereas previously described photorespiratory bypasses release four CO₂ molecules per two molecules of glycolate (22, 23), the BHAC is carbon neutral and maximally releases one CO₂ molecule in case OAA is decarboxylated into PEP (25). We note that the introduction of the BHAC into plant peroxisomes did not improve the CCP compared to WT (Table 1). This suggests that either streamlining OAA assimilation or reintegration of the produced C3-intermediate PEP and/or CO₂ into the CBBC will be the key to achieve the full potential of the BHAC. At current stage, however, pleiotropic effects of diffuse OAA metabolism by several routes (amino acid biosynthesis, TCA cycle, and PEP/pyruvate metabolism) and reduced 3-phosphoglycerate regeneration that lowers the photosynthetic efficiency likely mask the full potential of the BHAC (Fig. 4). Integrating the BHAC into kinetic- and genome-scale metabolic models will help to identify further engineering targets (20, 47–49). Finally, the construction of a synthetic C4 cycle based on BHAC-derived OAA, either in a single cell or spatially separated cycle between mesophyll- and bundle-sheath cells would allow to enhance carbon assimilation in plants (17, 50) (SI Appendix, Fig. S11). We note that using photorespiration as source of the synthetic C4 cycle would circumvent the need to establish PEPC-dependent CO₂ fixation in C3 plants, make an ATP-dependent regeneration of PEP dispensable, and ultimately conserve energy.

In summary, this work on engineering a functional BHAC into *Arabidopsis* is a starting point to turn a photorespiratory bypass into a synthetic C4 cycle, constituting a promising approach toward creating higher crop yields in the future.

Materials and Methods

Chemicals. D-erythro-BHA ((2R,3S)- β -hydroxyaspartate) was custom synthesized and determined to be >95% pure by NMR analysis (NewChem). DL-threo-BHA was purchased as racemic mixture (Sigma Aldrich).

Plasmid Construction. BHAC genes were codon optimized for expression in *A. thaliana* by gene synthesis (ThermoFisher Scientific) and matured for golden-gate cloning. All plasmids were generated with the MoClo tool kit, including vector backbones and genetic parts (51). Plasmids were sequenced by Sanger sequencing (Microsynth). Plasmids and primers used in this study are listed in SI Appendix, Tables S1 and S2, respectively.

BHAC Enzyme Activity Assays. BHAC enzyme activity was measured in total leaf protein extracts from 4-wk-old air-grown *Arabidopsis* plants. Purified recombinant BHAC enzymes were produced as described in ref. 25. The reaction mixture to assay AGAT activity contained 100 mM potassium phosphate buffer (pH = 7.5), 0.1 mM PLP, 0.2 mM NADH, 5 mM glyoxylate, 20 mM aspartate, 25 μ L of leaf extract, and 8.75 μ g NAD-dependent malate dehydrogenase (Sigma Aldrich). The reaction mixture to assay BHAA activity contained 100 mM potassium phosphate buffer (pH = 7.5), 0.1 mM PLP, 0.2 mM NADH, 0.5 mM MgCl₂, 5 mM glyoxylate, 10 mM glycine, 25 μ L of leaf extract, and 7 μ g purified BHAD and 7 μ g purified ISR enzyme. The reaction mixture to assay BHAD activity contained 100 mM potassium phosphate buffer (pH = 7.5), 0.1 mM PLP, 0.2 mM NADH, 2 mM erythro-BHA, 25 μ L of leaf extract, and 7 μ g purified ISR enzyme. The reaction mixture to assay ISR activity contained 100 mM potassium phosphate buffer (pH = 7.5), 0.1 mM PLP, 0.2 mM NADH, 5 mM glyoxylate, and 10 mM ¹⁵N-glycine, 50 μ L of leaf extract, and 7 μ g purified BHAA and BHAD enzyme. The formation of ¹⁵N-aspartate by ISR activity was confirmed by liquid chromatography with tandem mass spectrometry (LC-MS/MS). A detailed description of the LC-MS/MS method is provided in the SI Appendix, Text.

Plant Material and Cultivation Conditions. The *A. thaliana* ecotype *Col-0* and the *ggt1-1* mutant (29), deficient in the peroxisomal glutamate:glyoxylate aminotransferase 1 (GGT1) were used as reference backgrounds. Seeds were surface sterilized using the vapor-phase sterilization method (52). Seeds were grown on half-strength Murashige and Skoog medium (pH = 5.7) supplemented with 0.8% (wt/vol) agar. Seeds were cold stratified for 2 d at 4 °C. After germination, seedlings were grown for 14 d at 100 μ mol m⁻² · s⁻¹ light intensity at atmospheric CO₂ concentration (400 ppm) or in CO₂-enriched air (3,000 ppm) in 12-h light/12-h dark photoperiod prior transfer to soil.

Metabolite Profiling. For metabolite profiling, green tissue of 14-d-old seedlings was harvested by immediate quenching with liquid nitrogen at the middle of the light phase. A total of 50 mg leaf material was extracted as previously described (53) and analyzed by GC/MS Q-TOF (Agilent). For ion chromatography–mass spectrometry (IC/MS, Thermo Fisher Scientific), tissue was extracted as previously described (54). For relative quantification, metabolite peak areas were normalized to the internal extraction standard and the material fresh weight. A detailed description of the GC/MS Q-TOF and IC/MS methods and the respective data analysis is provided in the SI Appendix, Text.

Gas Exchange Measurements. Mature rosette leaves of 6-wk-old air-grown plants were used for gas exchange measurements. Measurements were performed using a LICOR6800 (Licor Bioscience) with a flow set to 300 μ mol s⁻¹, saturating light intensity of 1,000 μ mol m⁻² · s⁻¹, leaf temperature of 25 °C, and a vapor pressure deficit below 1.5 kPa. A/C_i curves were measured via stepwise changes in external CO₂ supply ranging from 0 to 1,600 μ bar. From the A/C_i curves the CO₂ compensation point was determined as x-intercept (36). The initial slope of the A/C_i curve was calculated in the linear range between 0 and 200 μ bar external CO₂, and the maximal assimilation rate (A_{\max}) above 1,000 μ bar CO₂ was determined. Dark respiration was determined by light response measurements at constant external CO₂ of 400 μ bar, and light intensities were stepwise reduced from 1,600 to 0 μ mol m⁻² · s⁻¹. The O₂ dependency of the CO₂ compensation point was determined by stepwise reducing the external CO₂ from 400 to 10 μ bar under an applied N₂-pressured air mixture at a ratio of 4:1, providing an estimated O₂ concentrations of 4%. The gas mixture was realized with the help two variable air flowmeters. The leaves were always allowed to adjust to the O₂ conditions for ~15 min.

Data Availability. Data analysis was performed in R. For analysis of gas exchange measurements, the “plantecophys” package was used (55). The data are summarized in [Datasets S1–S10](#). All other study data are included in the article and/or supporting information.

ACKNOWLEDGMENTS. We thank Raja Stracke, Elisabeth Klemp, Maria Graf, and Katrin Weber for excellent technical assistance and Nina Cortina for her contribution in developing the ISR MS method. Work in the laboratory of

A.P.M.W was funded by the German Research Foundation (DFG) under Germany’s Excellence Strategy (CEPLAS [Cluster of Excellence on Plant Science]), the iGRAD Plant Graduate School (IGK 2466), and European Union H2020 Project 862087-GAIN4CROPS. The CEPLAS metabolism and metabolomics laboratory is funded by the DFG under Germany’s Excellence Strategy (EXC-2048/1–Project 390686111). Work in the laboratory of T.J.E. was funded by the Max Planck Society and the DFG (SFB987 “Microbial diversity in environmental signal response”).

1. D. Tilman, C. Balzer, J. Hill, B. L. Befort, Global food demand and the sustainable intensification of agriculture. *Proc. Natl. Acad. Sci. U.S.A.* **108**, 20260–20264 (2011).
2. C. A. Jones, R. D. Sands, Impact of agricultural productivity gains on greenhouse gas emissions: A global analysis. *Am. J. Agric. Econ.* **95**, 1309–1316 (2013).
3. D. K. Ray, N. D. Mueller, P. C. West, J. A. Foley, Yield trends are insufficient to double global crop production by 2050. *PLoS One* **8**, e66428 (2013).
4. P. Pradhan, G. Fischer, H. van Velthuizen, D. E. Reusser, J. P. Kropp, Closing yield gaps: How sustainable can we be? *PLoS One* **10**, e0129487 (2015).
5. S. P. Long, A. Marshall-Colon, X.-G. Zhu, Meeting the global food demand of the future by engineering crop photosynthesis and yield potential. *Cell* **161**, 56–66 (2015).
6. E. T. Wurtzel *et al.*, Revolutionizing agriculture with synthetic biology. *Nat. Plants* **5**, 1207–1210 (2019).
7. A. P. M. Weber, A. Bar-Even, Update: Improving the efficiency of photosynthetic carbon reactions. *Plant Physiol.* **179**, 803–812 (2019).
8. T. Schwander, L. Schada von Borzyskowski, S. Burgener, N. S. Cortina, T. J. Erb, A synthetic pathway for the fixation of carbon dioxide in vitro. *Science* **354**, 900–904 (2016).
9. T. E. Miller *et al.*, Light-powered CO₂ fixation in a chloroplast mimic with natural and synthetic parts. *Science* **368**, 649–654 (2020).
10. M. Scheffen *et al.*, A new-to-nature carboxylation module to improve natural and synthetic CO₂ fixation. *Nat. Catal.* **4**, 105–115 (2021).
11. A. Bar-Even, E. Noor, N. E. Lewis, R. Milo, Design and analysis of synthetic carbon fixation pathways. *Proc. Natl. Acad. Sci. U.S.A.* **107**, 8889–8894 (2010).
12. M.-S. Roell, M. D. Zurbruggen, The impact of synthetic biology for future agriculture and nutrition. *Curr. Opin. Biotechnol.* **61**, 102–109 (2020).
13. C. A. Kerfeld, C. Aussignargues, J. Zarzycki, F. Cai, M. Sutter, Bacterial micro-compartments. *Nat. Rev. Microbiol.* **16**, 277–290 (2018).
14. J. H. Hennacy, M. C. Jonikas, Prospects for engineering biophysical CO₂ concentrating mechanisms into land plants to enhance yields. *Annu. Rev. Plant Biol.* **71**, 461–485 (2020).
15. U. Schlüter, A. P. M. Weber, Regulation and evolution of C₄ photosynthesis. *Annu. Rev. Plant Biol.* **71**, 183–215 (2020).
16. M. L. Schuler, O. Mantegazza, A. P. M. Weber, Engineering C₄ photosynthesis into C₃ chassis in the synthetic biology age. *Plant J.* **87**, 51–65 (2016).
17. M. Ermakova, F. R. Danila, R. T. Furbank, S. von Caemmerer, On the road to C₄ rice: Advances and perspectives. *Plant J.* **101**, 940–950 (2020).
18. B. J. Walker, A. VanLoocke, C. J. Bernacchi, D. R. Ort, The costs of photorespiration to food production now and in the future. *Annu. Rev. Plant Biol.* **67**, 107–129 (2016).
19. M. Eisenhut, M.-S. Roell, A. P. M. Weber, Mechanistic understanding of photorespiration paves the way to a new green revolution. *New Phytol.* **223**, 1762–1769 (2019).
20. D. L. Trudeau *et al.*, Design and in vitro realization of carbon-conserving photorespiration. *Proc. Natl. Acad. Sci. U.S.A.* **115**, E11455–E11464 (2018).
21. R. Kebeish *et al.*, Chloroplastic photorespiratory bypass increases photosynthesis and biomass production in *Arabidopsis thaliana*. *Nat. Biotechnol.* **25**, 593–599 (2007).
22. A. Maier *et al.*, Transgenic introduction of a glycolate oxidative cycle into *A. thaliana* chloroplasts leads to growth improvement. *Front. Plant Sci.* **3**, 38 (2012).
23. P. F. South, A. P. Cavanagh, H. W. Liu, D. R. Ort, Synthetic glycolate metabolism pathways stimulate crop growth and productivity in the field. *Science* **363**, eaat9077 (2019).
24. B.-R. Shen *et al.*, Engineering a new chloroplastic photorespiratory bypass to increase photosynthetic efficiency and productivity in rice. *Mol. Plant* **12**, 199–214 (2019).
25. L. Schada von Borzyskowski *et al.*, Marine Proteobacteria metabolize glycolate via the β -hydroxyaspartate cycle. *Nature* **575**, 500–504 (2019).
26. T. Lingner *et al.*, Identification of novel plant peroxisomal targeting signals by a combination of machine learning methods and in vivo subcellular targeting analyses. *Plant Cell* **23**, 1556–1572 (2011).
27. A. Dedonder, R. Rethy, H. Fredericq, M. Van Montagu, E. Krebbers, *Arabidopsis rbcS* genes are differentially regulated by light. *Plant Physiol.* **101**, 801–808 (1993).
28. A. Mitra, J. Han, Z. J. Zhang, A. Mitra, The intergenic region of *Arabidopsis thaliana cab1* and *cab2* divergent genes functions as a bidirectional promoter. *Planta* **229**, 1015–1022 (2009).
29. Y. Dellero, M. Lamothe-Sibold, M. Jossier, M. Hodges, *Arabidopsis thaliana ggt1* photorespiratory mutants maintain leaf carbon/nitrogen balance by reducing RuBisCO content and plant growth. *Plant J.* **83**, 1005–1018 (2015).
30. A. B. Cousins, I. Pracharoenwattana, W. Zhou, S. M. Smith, M. R. Badger, Peroxisomal malate dehydrogenase is not essential for photorespiration in *Arabidopsis* but its absence causes an increase in the stoichiometry of photorespiratory CO₂ release. *Plant Physiol.* **148**, 786–795 (2008).
31. A. R. Fernie, H. Bauwe, Wasteful, essential, evolutionary stepping stone? The multiple personalities of the photorespiratory pathway. *Plant J.* **102**, 666–677 (2020).
32. L. Charton, A. Plett, N. Linka, Plant peroxisomal solute transporter proteins. *J. Integr. Plant Biol.* **61**, 817–835 (2019).
33. P. J. Eastmond *et al.*, *Arabidopsis* uses two gluconeogenic gateways for organic acids to fuel seedling establishment. *Nat. Commun.* **6**, 6659 (2015).
34. S. Wulfert, S. Schilasky, S. Krueger, Transcriptional and biochemical characterization of cytosolic pyruvate kinases in *Arabidopsis thaliana*. *Plants* **9**, 353 (2020).
35. U. Schlüter *et al.*, Photosynthesis in C₃-C₄ intermediate *Morandia* species. *J. Exp. Bot.* **68**, 191–206 (2017).
36. T. D. Sharkey, C. J. Bernacchi, G. D. Farquhar, E. L. Singaas, Fitting photosynthetic carbon dioxide response curves for C₃ leaves. *Plant Cell Environ.* **30**, 1035–1040 (2007).
37. A. J. Bloom, Photorespiration and nitrate assimilation: A major intersection between plant carbon and nitrogen. *Photosynth. Res.* **123**, 117–128 (2015).
38. C. M. Pérez-Delgado, M. García-Calderón, A. J. Márquez, M. Betti, Reassimilation of photorespiratory ammonium in *Lotus japonicus* plants deficient in plastidic glutamine synthetase. *PLoS One* **10**, e0130438 (2015).
39. C. Blume, J. Ost, M. Mühlenbruch, C. Peterhänsel, M. Laxa, Low CO₂ induces urea cycle intermediate accumulation in *Arabidopsis thaliana*. *PLoS One* **14**, e0210342 (2019).
40. M. Linka, A. P. M. Weber, Shuffling ammonia between mitochondria and plastids during photorespiration. *Trends Plant Sci.* **10**, 461–465 (2015).
41. C. J. Schultz, G. M. Coruzzi, The aspartate aminotransferase gene family of *Arabidopsis* encodes isoenzymes localized to three distinct subcellular compartments. *Plant J.* **7**, 61–75 (1995).
42. M. Kirma, W. L. Araújo, A. R. Fernie, G. Galili, The multifaceted role of aspartate-family amino acids in plant metabolism. *J. Exp. Bot.* **63**, 4995–5001 (2012).
43. S. Ravel *et al.*, Methionine metabolism in plants: Chloroplasts are autonomous for de novo methionine synthesis and can import S-adenosylmethionine from the cytosol. *J. Biol. Chem.* **279**, 22548–22557 (2004).
44. R. Boldt *et al.*, D-GLYCERATE 3-KINASE, the last unknown enzyme in the photorespiratory cycle in *Arabidopsis*, belongs to a novel kinase family. *Plant Cell* **17**, 2413–2420 (2005).
45. L. M. Voll *et al.*, The photorespiratory *Arabidopsis shm1* mutant is deficient in SHM1. *Plant Physiol.* **140**, 59–66 (2006).
46. M. Eisenhut *et al.*, *Arabidopsis* A BOUT DE SOUFFLE is a putative mitochondrial transporter involved in photorespiratory metabolism and is required for meristem growth at ambient CO₂ levels. *Plant J.* **73**, 836–849 (2013).
47. L. J. Sweetlove, R. G. Ratcliffe, Flux-balance modeling of plant metabolism. *Front. Plant Sci.* **2**, 38 (2011).
48. A. Küken, Z. Nikoloski, Computational approaches to design and test plant synthetic metabolic pathways. *Plant Physiol.* **179**, 894–906 (2019).
49. A. Matuszyńska, N. P. Saadat, O. Ebenhöf, Balancing energy supply during photosynthesis – a theoretical perspective. *Physiol. Plant.* **166**, 392–402 (2019).
50. I. Jurić, J. M. Hibberd, M. Blatt, N. J. Burroughs, Computational modelling predicts substantial carbon assimilation gains for C₃ plants with a single-celled C₄ biochemical pump. *PLoS Comput. Biol.* **15**, e1007373 (2019).
51. C. Engler *et al.*, A golden gate modular cloning toolbox for plants. *ACS Synth. Biol.* **3**, 839–843 (2014).
52. S. J. Clough, A. F. Bent, Floral dip: A simplified method for agrobacterium-mediated transformation of *Arabidopsis thaliana*. *Plant J.* **16**, 735–743 (1998).
53. O. Fiehn *et al.*, Metabolite profiling for plant functional genomics. *Nat. Biotechnol.* **18**, 1157–1161 (2000).
54. S. Arrivault *et al.*, Use of reverse-phase liquid chromatography, linked to tandem mass spectrometry, to profile the Calvin cycle and other metabolic intermediates in *Arabidopsis* rosettes at different carbon dioxide concentrations. *Plant J.* **59**, 826–839 (2009).
55. R. A. Duursma, Plantecophys—An R package for analysing and modelling leaf gas exchange data. *PLoS One* **10**, e0143346 (2015).